

# PHYSICAL REVIEW C

## NUCLEAR PHYSICS

THIRD SERIES, VOLUME 41, NUMBER 3

MARCH 1990

### RAPID COMMUNICATIONS

*The Rapid Communications section is intended for the accelerated publication of important new results. Manuscripts submitted to this section are given priority in handling in the editorial office and in production. A Rapid Communication in Physical Review C may be no longer than five printed pages and must be accompanied by an abstract. Page proofs are sent to authors.*

#### Three paths for intermediate-mass fragment formation at a near-onset excitation energy of 1.3 MeV/nucleon

J. Boger, S. Kox,\* G. Auger,† J. M. Alexander, and A. Narayanan

*Department of Chemistry, State University of New York at Stony Brook, Stony Brook, New York 11794-3400*

M. A. McMahan

*Lawrence Berkeley Laboratory, Berkeley, California 94720*

D. J. Moses and M. Kaplan

*Department of Chemistry, Carnegie Mellon University, Pittsburgh, Pennsylvania 15213*

G. P. Gilfoyle

*Department of Physics, University of Richmond, Richmond, Virginia 23173*

(Received 8 December 1989)

Intermediate-mass fragments of  $4 \leq Z \leq 17$  have been studied from the reaction  $640 \text{ MeV } ^{86}\text{Kr} + ^{63}\text{Cu}$ . Inclusive energy and angular distribution measurements have been made as well as coincidence measurements with fissionlike fragments of  $18 \leq Z \leq 40$ . The coincidence configuration was such that two-body exit channels were excluded; nevertheless, heavy fragments were recorded both in plane and out of plane with respect to light fragments of  $4 \leq Z \leq 10$ . Three mechanisms have been identified for intermediate-mass fragment production. The dominant pathway for all intermediate-mass fragments is a two-body breakup of fission or evaporationlike character. A second pathway for  $Z \leq 10$  is intermediate-mass fragment ejection from the composite nucleus followed by sequential fission. The third path is a simultaneous ternary breakup for  $4 \leq Z \leq 9$  that resembles ternary alpha-accompanied fission at low energies.

The formation of intermediate-mass fragments (IMF's) with atomic numbers of  $\approx 3-15$ , is of great current interest.<sup>1</sup> This interest stems largely from the expectation that simultaneous multi-fragment emission might be a new reaction mechanism in violent heavy ion collisions. However, it is not easy to make a clearcut identification for such a multi-fragmentation process as distinct from sequential binary breakups, especially at high incident energies with a wide range of energy depositions. One can expect that the mechanisms for IMF formation will be more easily separable for relatively low energies, near the onset of their production, and where essentially complete fusion is the major reaction class. In an earlier study<sup>2</sup> of the reaction  $336 \text{ MeV } ^{40}\text{Ar} + ^{\text{nat}}\text{Ag} \rightarrow ^{149}\text{Tb}^*$  ( $E^* = 194 \text{ MeV}$ ), we found cross sections of  $\sim 2-10 \text{ mb}$  for evapora-

tionlike (or fissionlike) fragments of  $Z = 3, 4, \dots, 9$ . These small cross sections indicated IMF production at a near-onset excitation energy. In this work we have chosen the matched reaction  $640 \text{ MeV } ^{86}\text{Kr} + ^{63}\text{Cu} \rightarrow ^{149}\text{Tb}^*$  ( $E^* = 194 \text{ MeV}$ ). With reversed kinematics the IMF's have higher kinetic energies and higher counting rates, while the reactions with largest energy deposition still follow essentially complete fusion.

The experimental setup consisted of one small gas ionization telescope (GT), two similar, but larger gas telescopes<sup>3</sup> (GASP's), and four Si solid state telescopes (SST's). Intermediate-mass fragments ( $4 \leq Z \leq 17$ ) were detected in the gas telescopes in singles and in coincidence with fissionlike fragments ( $18 \leq Z \leq 40$ ), and with  $^1\text{H}$  and  $^4\text{He}$  in the SST's. In this work we will focus

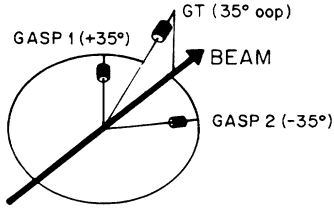


FIG. 1. Primary arrangement of the gas ionization detectors for intermediate-mass fragments ( $4 \leq Z \leq 17$ ) and fission fragments ( $18 \leq Z \leq 40$ ).

on the inclusive and exclusive data for IMF's and heavy fragments as recorded by the gas ionization telescopes. Results for fragment-particle coincidences and the light particles (inclusive and exclusive) will be published elsewhere. These data indicate that both IMF's and light-charged particles are largely produced after essentially complete fusion into a composite nucleus. In the primary configuration, shown in Fig. 1, each telescope was placed at  $\theta_{\text{lab}} = 35^\circ$ , two in the horizontal plane ( $\pm 35^\circ$ ) and one in the vertical plane. Subsequently, the table was rotated to obtain inclusive angular and energy distributions. Measurements were also made with a C target to test for the possible role of impurities on the Cu target. Energy and solid angle calibrations were based on elastic scattering of 142 and 158 MeV  $^{20}\text{Ne}$  beams by a thin Au target and on alpha-radioactive sources. Individual  $Z$  values were resolved for  $4 \leq Z \leq 17$ , and fusion fission or fission-like fragments were recorded as one group of  $18 \leq Z \leq 40$ .

In Fig. 2 we show inclusive c.m. kinetic energy spectra for IMF's of  $10 \leq Z \leq 15$  as obtained from detectors at  $\theta_{\text{lab}} = 35^\circ$ . Final product  $Z$  values were uniquely identified, and the average primary  $Z$  and  $A$  values were es-

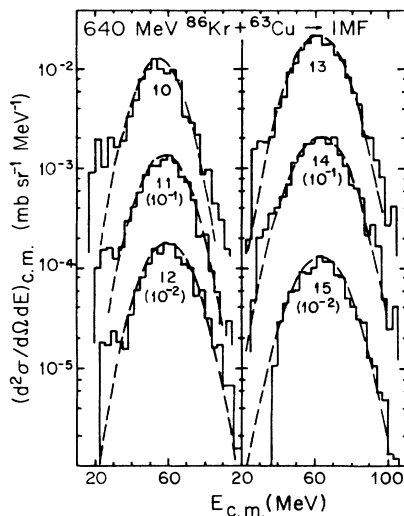


FIG. 2. Inclusive energy spectra (c.m.) for primary fragments (multiplying factors in parantheses) corresponding to the observed  $Z$  values of 10–15 ( $\theta_{\text{lab}} = 35^\circ$ , all detectors). Average primary masses were estimated to be 23.2, 26.7, 29.0, 31.3, 33.6, and  $35.8\mu$ . The dashed curves are fitted Gaussians.

timated from the separate determination of  $^1\text{H}$  and  $^4\text{He}$  in coincidence with the IMF's.<sup>4</sup> The major property of these energy spectra is their broad, near-Gaussian shape with standard deviations of  $\approx 20\%$  of the mean value. These spectra were also used to deduce total kinetic energies in two-body breakup, as discussed below.<sup>4</sup>

In Fig. 3 we show both inclusive and exclusive spectra for  $4 \leq Z \leq 9$ . No fragment-fragment coincidences were observed for the IMF's of  $11 \leq Z \leq 17$ . First, look at the solid histograms that give the singles spectra. We see that the shapes deviate from the Gaussian form rather strongly at low energies. There is a distinct low-energy shelf that becomes increasingly important with decreasing  $Z$ . The short-dashed and long-dashed histograms show IMF spectra recorded in coincidence with a heavy, fissionlike fragment (HF) of  $18 \leq Z \leq 40$ , first in plane (GASP 1,2) and then out of plane (GASP, GT) with each detector at  $35^\circ$  (see Fig. 1). An essential point to realize about all of these fragment-fragment coincidence spectra is that they do *not* correspond to two-body exit channels. The vector diagram in Fig. 4(a) shows that typical recoil angles are  $\leq 10^\circ$  for the hypothetical heavy-fragment partners of two-body breakup. These recoil angles are all much too small to be accepted by the configuration shown in Fig. 1.

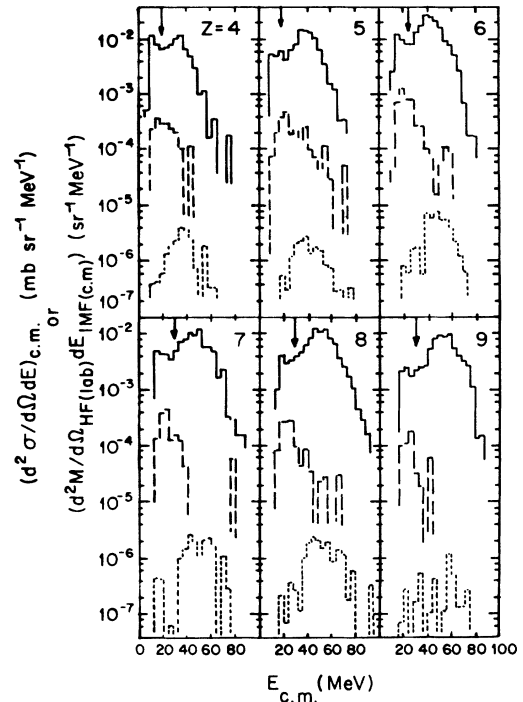


FIG. 3. Energy spectra (c.m.) for primary fragments for observed  $Z$  values of 4–9 ( $\theta_{\text{lab}} = 35^\circ$ ). Solid histograms for inclusive data; short-dashed for in-plane coincidences (GASP 1,2); long-dashed for out-of-plane coincidences (GASP, GT). Average primary masses were estimated to be 9.5, 11.8, 14.1, 16.3, 18.6, and 20.9, respectively. For each  $Z$  the boundary between groups is indicated. For differential multiplicities from the coincidence data we show

$$d^2 M / d\Omega_{\text{HF(lab)}} dE_{\text{IMF(c.m.)}}$$

$$= (d^3 \sigma / d\Omega_{\text{HF(lab)}} d\Omega_{\text{IMF(c.m.)}} dE_{\text{IMF(c.m.)}}) / (d\sigma / d\Omega_{\text{IMF(c.m.)}}).$$

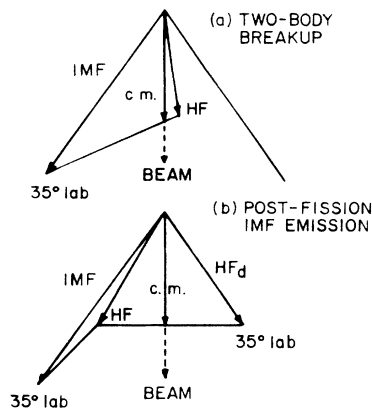


FIG. 4. In-plane vector diagrams for  $Z=6$ : (a) two-body breakup and (b) post-fission emission of  $Z=6$  fragment from fully-accelerated, mass-symmetric fission fragments. Average velocity vectors are indicated for the IMF, the c.m., and the detected heavy fragment  $HF_d$ . Asymmetry in the HF vectors in (b) results from kinematic selectivity of the detector geometry.

Therefore, we must be observing three (or more) body reactions in these fragment-fragment coincidences. Chance coincidence corrections have been subtracted. By moving the edge of one GASP detector to  $7.5^\circ$ , we did observe the two-body breakups, but could not measure their cross sections directly.

It is particularly interesting that the shapes of the in-plane coincidence spectra ( $4 \leq Z \leq 10$ ) are very similar to the broad, high-energy peaks in the singles spectra, while the out-of-plane spectra seem to reflect the low-energy shelf observed in the singles. This contrast suggests the possibility of two separate mechanisms so we have divided the IMF's into two groups of low and high energy, with the boundaries indicated in Fig. 3. One can examine these groups with an eye towards four mechanistic paths for IMF production: (a) simple two-body breakup, (b) IMF ejection from the composite nucleus followed by fission, (c) IMF ejection in a three-body simultaneous breakup, and (d) IMF ejection from fission fragments after their formation and acceleration.

Pathways (a) and (b) are the most simple to consider; in both, the IMF's are expected to exhibit total kinetic energy (TKE) values driven by the Coulomb repulsion of very asymmetric, two-body, fissionlike breakup.<sup>2,5</sup> Figure 5 compares the mean TKE values (inclusive data, high-energy peak only) to values calculated from a macroscopic model.<sup>5,6</sup> It is clear that there is a rather close correspondence that suggests ejection of the IMF's from the composite nucleus. The strong similarity of the singles spectra and the in-plane coincidence spectra (Fig. 3) suggests that these coincidences (in-plane only) correspond to IMF ejection followed much later by fission.

Additional evidence for this conclusion can be obtained from the observed multiplicities for fission products HF ( $18 \leq Z \leq 40$ ) with respect to the IMF's. Table I gives values for preliminary multiplicities (PM) for each energy group, defined as follows:

$$PM = 2\pi(d^2\sigma/d\Omega_{IMF}d\Omega_{HF})/(d\sigma/d\Omega_{IMF}). \quad (1)$$

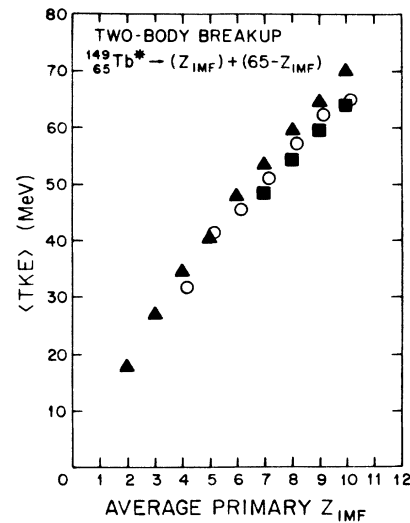


FIG. 5. Average total kinetic energy TKE vs primary fragment  $Z$ :  $\blacktriangle$ , calculated upper limit from a macroscopic fission model, Ref. 5;  $\blacksquare$ , calculated lower limit from a macroscopic fission model, Ref. 6;  $\circ$ , experimental values from this work for the high-energy group only.

We term these preliminary multiplicities because the factor  $2\pi$  (i.e.,  $4\pi \text{ sr}/2$  fragments) has been used to give crude angular integration for a hypothetical isotropic fission process in the c.m. For the high-energy group of IMF's there are two important results given in Table I: (a) the ratio of in-plane to out-of-plane coincidences is

TABLE I. IMF-fission fragment multiplicities (PM) and angle integrated cross sections ( $\langle PM \rangle \sigma$ ).

$Z_{IMF}$	PM <sup>a</sup> (in plane)	PM <sup>a</sup> (out of plane)	$\langle PM \rangle \sigma_{IMF}^b$ (mb)
High-energy group			
4	$0.12 \pm 0.02$	$< 0.02$	0.36
5	$0.08 \pm 0.01$	$0.02 \pm 0.01$	0.26
6	$0.11 \pm 0.01$	$0.02 \pm 0.02$	0.68
7	$0.10 \pm 0.02$	$< 0.01$	0.27
8	$0.07 \pm 0.01$	$0.03 \pm 0.04$	0.29
9	$0.05 \pm 0.01$	$0.01 \pm 0.01$	0.10
10	$0.07 \pm 0.01$	$0.01 \pm 0.01$	0.22
Low-energy group			
4	$0.03 \pm 0.01$	$0.16 \pm 0.04$	0.14
5	$0.05 \pm 0.02$	$0.24 \pm 0.07$	0.10
6	$0.05 \pm 0.02$	$0.19 \pm 0.03$	0.16
7	$0.02 \pm 0.01$	$0.16 \pm 0.04$	0.07
8	$0.03 \pm 0.02$	$0.14 \pm 0.03$	0.06
9	$0.07 \pm 0.03$	$0.15 \pm 0.04$	0.05
10	$0.06 \pm 0.03$	$0.09 \pm 0.03$	0.03

<sup>a</sup>From Eq. (1).

<sup>b</sup> $\langle PM \rangle$  is the average of in-plane and out-of-plane values;  $\sigma_{IMF}$  is the inclusive cross section for the relevant IMF group. Relative uncertainties are shown for the PM values; absolute uncertainties depend on the crude angular integration and may reach a factor of 2.

very large and (b) the average multiplicities  $\langle PM \rangle$  are small,  $\leq 10\%$ , and tend to decrease with increasing  $Z$ . These low average multiplicities indicate that only a small fraction of the high-energy IMF production is accompanied by fission fragments of  $18 \leq Z \leq 40$ . Therefore, the bulk of the inclusive IMF's can be attributed to very mass-asymmetric two-body breakup. The strong in-plane preference for fragments and high-energy IMF's suggests that both the IMF breakup and the fissionlike breakup occur preferentially perpendicular to the spin of the composite system. And, again, the similar inclusive and exclusive energy spectra indicate that the IMF is emitted prior to fission and is essentially unperturbed by its later occurrence.

Turning now to the low-energy IMF group in Fig. 3 and Table I, we see very different behavior. These low-energy fragments have preferred emission out of plane with respect to the fission products. Their average multiplicities seem to be larger than those for the high-energy group and they are roughly constant with increasing  $Z$ . This behavior suggests that the low-energy IMF production does not occur prior to fission, and one should consider simultaneous or post-fission ejection. The vector diagram in Fig. 4(b) has been drawn to illustrate the expected kinematics for in-plane coincidences in post-scission IMF ejection. Clearly this kinematic behavior shown in Fig. 4(b) is completely at variance with the data. The post-fission IMF's would be preferentially detected in plane and with velocities larger than the prefission IMF's.

What about simultaneous ternary breakup into an IMF of  $Z \leq 10$  and two fission products of  $18 \leq Z \leq 40$ ? If this process is similar to ternary fission (i.e., alpha-particle accompanied fission) at low energies, then the IMF's

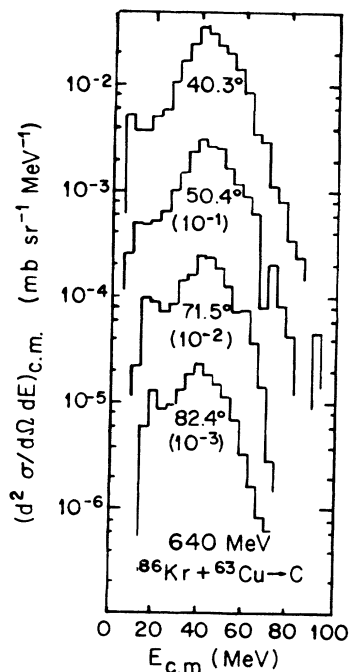


FIG. 6. Inclusive energy spectra (c.m.) vs average c.m. angle for primary fragments corresponding to final  $Z=6$  (C).

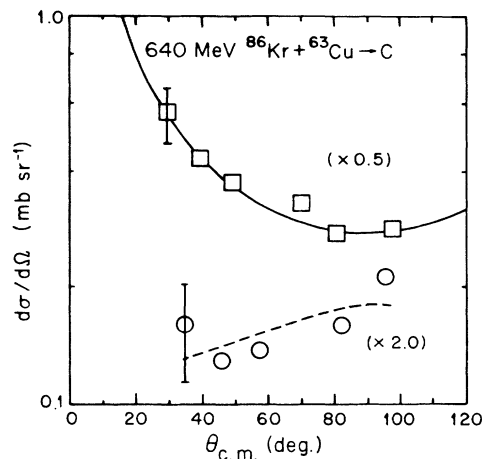


FIG. 7. Angular distributions for final  $Z=6$  (C);  $\square$ , high-energy group with  $E_{c.m.} \geq 24$  MeV;  $\circ$ , low-energy group with  $16 \leq E_{c.m.} \leq 24$  MeV. Solid line follows  $1/\sin\theta_{c.m.}$ ; dashed line is a guide to the eye.

would be expected to be emitted mainly perpendicular to the scission axis.<sup>7-9</sup> For the geometry of this experiment, detection of such emission would be favored for the out-of-plane configuration in Fig. 1 and strongly disfavored for the in-plane configuration. Also, the average energy of the IMF would be smaller than that for prescission emission because the Coulomb forces from the two heavy fragments would partially cancel in their action on an IMF in the middle.<sup>7-9</sup> Figure 3 and Table I do indicate both low energies and out-of-plane preference for this second group of IMF's. Therefore, we associate the low-energy IMF

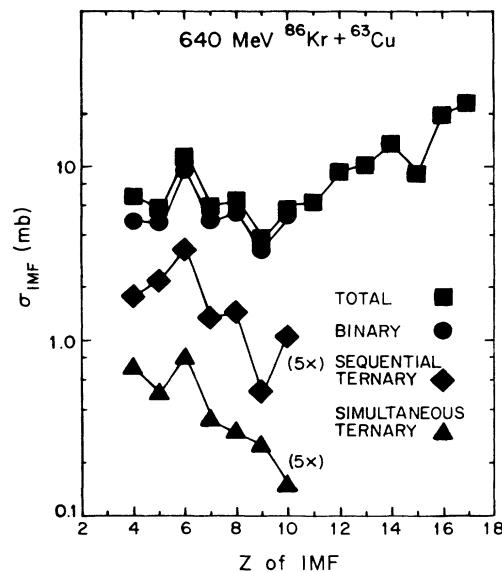


FIG. 8. Angle integrated cross sections vs final fragment  $Z$ ;  $\blacksquare$ , inclusive cross sections (thresholds shown in Figs. 2 and 3);  $\bullet$ , high-energy group produced in two-body breakup only;  $\blacklozenge$ , high-energy group in coincidence with sequential fission ( $18 \leq Z \leq 40$ );  $\blacktriangle$ , low-energy group emitted in simultaneous ternary breakups.

group with a simultaneous ternary breakup mechanism.

In this experiment we also made inclusive IMF measurements (in GASP 2) at several angles as shown in Fig. 6 for one case. The shapes of these spectra indicate a growth in the importance of the low-energy shelf as one moves from forward angles toward  $90^\circ$ . Again, we have divided the differential cross sections into high- and low-energy groups, and their angular distributions are shown in Fig. 7. The high-energy group has the characteristic forward-backward peaking (approximately  $1/\sin\theta_{c.m.}$ ) of strongly spin driven fission or evaporation processes. This is consistent with a predominantly binary breakup, unassociated with fission ( $18 \leq Z \leq 40$ ). The low-energy group seems to exhibit a preference for sideways emission in the c.m. These differential cross sections were taken for  $16 \leq E_{c.m.} \leq 24$  MeV, and are much more subject to experimental errors than are those for the high-energy group ( $E_{c.m.} \geq 24$  MeV). Nevertheless, the qualitative feature of sideways emission is strongly suggested. If these low-energy IMF's were predominantly emitted perpendicular to the forward-backward-peaked fragments of  $18 \leq Z \leq 40$ , then they would be side peaked. It is not possible for us to take this suggestion further now because our angular coverage was rather limited. Another experiment has been designed to pursue this point.<sup>10</sup>

In Fig. 8 we summarize the IMF cross sections from this experiment. The inclusive cross sections are rather flat at  $\approx 6$  mb for  $4 \leq Z \leq 10$ , with the commonly observed enhancement for  $Z=6$  and deficiency for  $Z=9$ . Then they gradually increase with  $Z$  as one moves toward symmetric fission. In contrast, there is a substantial decrease with increasing  $Z$  for the cross sections of both

high-energy and low-energy groups in coincidence with fission ( $18 \leq Z \leq 40$ ). Here the relative coincidence cross sections are much more indicative than the absolute values because of uncertainties in the crude angular integrations. Nevertheless, it is clear that the predominant path for IMF production is a binary breakup without any associated fragment of  $18 \leq Z \leq 40$ . In fact, no three-body exit channels were observed for  $Z > 10$ .

To summarize, in this study we have identified three mechanisms for IMF production in the reaction  $640 \text{ MeV } ^{86}\text{Kr} + ^{63}\text{Cu}$ . The dominant path for  $4 \leq Z \leq 17$  is a simple two-body breakup with fission or evaporationlike character. There is also IMF formation for  $4 \leq Z \leq 10$  in coincidence with fissionlike fragments of  $18 \leq Z \leq 40$ . We have divided these IMF's into a high-energy group and a low-energy group. The former is attributed to ejection from the composite nucleus prior to scission; the latter is attributed to simultaneous ternary breakup. These separate processes offer very interesting probes for the dynamics of reactions involving large spins and energies.

We want to thank N. N. Ajitanand, N. Carjan, A. Elmaani, M. T. Magda, and G. Williams for suggestions and helpful discussions. W. Rathbun was particularly helpful with the data acquisition system and the operating staff of the LBL SuperHILAC was most efficient. This research was supported by the Office of High Energy and Nuclear Physics of the United States Department of Energy and the Centre National de la Recherche Scientifique of France.

\*Permanent address: Institut des Sciences Nucléaires, Université de Grenoble 1, 38026 Grenoble CEDEX, France.

<sup>†</sup>Permanent address: Grand Accélérateur National d'Ions Lourds, Boîte Postale No. 5027, 14021 Caën CEDEX, France.

<sup>1</sup>Proceedings of the Third International Conference on Nucleus-Nucleus Collisions, Saint-Malo, France, 1988, edited by C. Detraz *et al.* [Nucl. Phys. A **488**, (1988)]; L. G. Moretto and G. J. Wozniak, in Proceedings of the International School of Physics "Enrico Fermi" Summer Course CXII, Varenna, 1989; Lawrence Berkeley Laboratory Report LBL-27502, and references therein.

<sup>2</sup>L. C. Vaz, D. Logan, J. M. Alexander, E. Duek, D. Guerreau, L. Kowalski, M. F. Rivet, and M. S. Zisman, Z. Phys. A **311**, 89 (1983).

<sup>3</sup>These detectors were designed and built at Lawrence Berkeley Laboratory with the guidance of G. Wozniak and L. Sobotka.

<sup>4</sup>A mass-energy balance has been estimated from measured pre- and post-scission  $^1\text{H}$  and  $^4\text{He}$  multiplicities along with evaporation calculations for the ratios of neutron to alpha-

particle emission. In this way both primary and final masses were estimated for each IMF as well as the mass of the fissioning nucleus.

<sup>5</sup>N. Carjan and J. M. Alexander, Phys. Rev. C **38**, 1692 (1988).

<sup>6</sup>N. Carjan, *International Symposium on Heavy-Ion Reaction Dynamics in the Tandem Energy Region, Hitachi, Japan 1988* (Report No. 8826, Centre d'Etudes Nucleaires de Bordeaux-Gradignan).

<sup>7</sup>R. Vandenbosch and J. R. Huizenga, *Nuclear Fission* (Academic, New York, 1973), Chap. 14 and references therein.

<sup>8</sup>E. Duek, N. N. Ajitanand, J. M. Alexander, D. Logan, M. Kildir, L. Kowalski, L. C. Vaz, D. Guerreau, M. S. Zisman, and M. Kaplan, Phys. Lett. **131B**, 297 (1983).

<sup>9</sup>R. Lacey, N. N. Ajitanand, J. M. Alexander, D. M. deCastro Rizzo, G. F. Peaslee, L. C. Vaz, M. Kaplan, M. Kildir, G. LaRana, D. J. Moses, W. E. Parker, D. Logan, M. S. Zisman, P. DeYoung, and L. Kowalski, Phys. Rev. C **37**, 2540 (1988).

<sup>10</sup>M. Kaplan *et al.* (unpublished).